Research Square

Preprints are preliminary reports that have not undergone peer review.
They should not be considered conclusive, used to inform clinical practice,
or referenced by the media as validated information.

Integrated RNA-seq and ATAC-seq profiling for assessing chemically induced inflammatory responses in human TK6 cells

Keigo Yamakita
Chiba University
Manabu Yasui
National Institute of Health Sciences
Masamitsu Honma
National Institute of Health Sciences
Kei-ichi Sugiyama
National Institute of Health Sciences
Ryoji Fujiki
Shimane University
Atsushi Kaneda
Chiba University
Kiyoe Ura
Chiba University
Akira Sassa
a-sassa@chiba-u.jp

Chiba University

Research Article

Keywords: Inflammation, chromatin accessibility, RNA-seq, ATAC-seq, TK6

Posted Date: October 30th, 2026

DOI: https://doi.org/10.21203/rs.3.rs-11215949/v1

License: This work is licensed under a Creative Commons Attribution 4.0 International License.
Read Full License

Additional Declarations: No competing interests reported.

Abstract

Background

Chemical exposure can exert biological effects not only through genetic alterations but also by changing gene regulation and chromatin states. Inflammation is a key cellular response to diverse chemical stresses, and immune cells control activation and inflammatory gene programs through dynamic chromatin remodeling; moreover, chronic inflammation and immunosuppression are recognized key characteristics of carcinogens. However, how chemically induced transcriptional responses are coordinated with changes in chromatin accessibility remains incompletely understood. Here, we investigated whether integrating transcriptomic and chromatin accessibility profiling could provide a molecular framework for assessing chemically induced inflammatory responses. To do so, human TK6 cells, an immune-lineage cell line widely used in regulatory genotoxicity testing, were exposed for 24h to the non-genotoxic tumor promoter 12-O-tetradecanoylphorbol-13-acetate (TPA), allowed to recover for up to 7 days before being analyzed by RNA sequencing (RNA-seq) and assay for transposase-accessible chromatin using sequencing (ATAC-seq).

Results

TPA induced time-dependent transcriptional changes that persisted after chemical removal. Upregulated genes were enriched in immune- and inflammation-related processes, including leukocyte and lymphocyte activation and cytokine production. ATAC-seq revealed extensive chromatin remodeling that increased progressively during the post-exposure period: the total number of differentially accessible regions rose from 6,488 immediately after exposure to 11,364 and 12,710 on Days 3 and 7, respectively. Integrated RNA-seq and ATAC-seq analysis showed that the proportion of upregulated genes accompanied by increased chromatin accessibility rose from 32.7% on Day 0 to 50.1% and 46.3% on Days 3 and 7, respectively. Concordance among downregulated genes increased more markedly, from 8.7% on Day 0 to 26.1% on Day 3 and 39.6% on Day 7. Concordant changes included inflammation-related genes associated with susceptibility to human disease, including *TNFSF4, CSF2, and SELL*.

Conclusions

These findings show that TPA induces sustained transcriptional and chromatin states that continue to remodel after chemical removal. Integrated RNA-seq and ATAC-seq profiling identifies coordinated molecular responses that transcriptomic analysis alone does not capture. These concordant RNA–ATAC changes, particularly at disease-associated inflammatory genes, may provide candidate molecular indicators for mechanistically informed assessment of chemically induced inflammatory and non-genotoxic effects.

Introduction

Cells are continuously challenged by a broad range of exogenous and endogenous stressors. Through diverse mechanisms, these agents can disrupt cellular functions and homeostasis, thereby contributing to aging, carcinogenesis, and the development or progression of various diseases. Genotoxicity is one major mechanism underlying such adverse effects. Genotoxic agents act directly or indirectly on genomic DNA or chromosomes, causing DNA damage that can subsequently produce genetic alterations such as mutations and chromosomal abnormalities [1]. However, the biological effects of chemicals are not limited to changes in DNA sequence. Chemicals can also perturb epigenetic regulatory mechanisms, including DNA methylation, histone modifications, and consequent changes in chromatin organization, thereby inducing sustained or long-lasting alterations in gene expression [2–5]. Chemically induced epigenetic alterations may arise directly through effects on epigenetic regulators, such as DNA methyltransferases and histone-modifying enzymes, or indirectly through changes in cellular metabolism, redox balance, and energy homeostasis [6]. For example, metabolites such as acetyl-CoA, S-adenosylmethionine, α-ketoglutarate, and NAD+ serve as substrates or cofactors for histone acetylation, DNA and histone methylation, demethylation, and deacetylation, directly linking cellular metabolic states to chromatin regulation [7]. Thus, chemical exposure can produce closely interconnected metabolic and epigenetic alterations whose biological consequences are likely mediated through complex molecular networks rather than a single molecular target.

Changes in metabolic control, genome integrity, and epigenetic regulation are ultimately reflected in gene expression programs through altered chromatin states [8, 9]. Thus, chromatin structure serves as an important regulatory platform that integrates diverse intracellular and extracellular stress signals and translates them into transcriptional responses. Among these responses, inflammation is a representative biological process triggered by disruption of cellular homeostasis. Oxidative stress, mitochondrial dysfunction, metabolic reprogramming, endoplasmic reticulum stress, DNA damage, and epigenetic alterations can activate innate immune signaling and inflammation-related transcriptional pathways while simultaneously altering chromatin accessibility and reshaping inflammatory gene expression programs [10]. Although inflammatory responses are essential for host defense, tissue repair, and restoration of tissue homeostasis, their excessive or persistent activation is closely associated with carcinogenesis, cellular and organismal aging, autoinflammatory and autoimmune diseases, and many other pathological conditions [11]. Comprehensive characterization of inflammation-related transcriptional responses together with their underlying chromatin-state changes is therefore important for assessing potential chemical hazards and mechanisms of action [12].

Pathogen-associated molecular patterns (PAMPs) and damage-associated molecular patterns (DAMPs) can both initiate inflammatory responses. DAMPs include ATP, mitochondrial components, and cytosolic nucleic acids that are released or generated during cellular stress or tissue damage [13, 14]. These signals are detected through pattern-recognition receptors and intracellular sensing pathways such as the cGAS–STING pathway [15]. Inflammatory transcription can also be activated directly by intracellular stresses, including oxidative stress, endoplasmic reticulum stress, and DNA damage, through pathways involving NF-κB, AP-1, JAK–STAT, and interferon regulatory factors [16, 17]. Thus, cellular stresses with distinct molecular origins can converge on reprogramming of inflammatory gene expression. Excessive

activation or dysregulation of these networks is associated with numerous pathological conditions. These include autoimmune and autoinflammatory diseases such as systemic lupus erythematosus, Aicardi–Goutières syndrome, and rheumatoid arthritis, together with cancer- and aging-associated chronic inflammation [18–20]. In response to chemical and other cellular stresses, genes linked to disease susceptibility and disease-related inflammatory states can undergo dynamic transcriptional regulation that may be accompanied by altered chromatin accessibility [21–23]. Chromatin remodeling may therefore provide an important regulatory layer that determines how disease-associated inflammatory genes respond to stress [24, 25].

In the present study, inflammation was used as a potential indicator of chemically induced biological effects, and we comprehensively examined associated changes in gene expression and chromatin dynamics. The experiments used human lymphoblastoid TK6 cells, which retain functional p53, have a relatively stable karyotype, and are widely used not only for genotoxicity testing but also for evaluating broader chemical effects [26–29]. We selected 12-O-tetradecanoylphorbol-13-acetate (TPA) as the model compound because this prototypical non-genotoxic tumor promoter and phorbol ester activates protein kinase C signaling and elicits broad transcriptional and inflammatory responses [30–32]. Genome-wide, time-resolved RNA sequencing (RNA-seq) and assay for transposase-accessible chromatin using sequencing (ATAC-seq) were then integrated to characterize these responses. Using this approach, we asked whether combined analysis of gene expression and chromatin states can provide a molecular framework for evaluating inflammatory effects associated with chemical stress.

Materials and Methods

Cell culture

The human lymphoblastoid cell line TSCE5, an isogenic derivative of TK6, was used in this study [33]. Cells were cultured at 37°C, 5% CO_2, and 100% humidity in RPMI-1640 medium (Nacalai Tesque) supplemented with 10% heat-inactivated horse serum (Gibco), 100 U/mL penicillin, 100 µg/mL streptomycin, and 200 µg/mL sodium pyruvate.

Chemical treatment

12-O-tetradecanoylphorbol-13-acetate (TPA) was purchased from Wako Pure Chemical Industries Ltd. (Osaka, Japan) and prepared in 100% ethanol (EtOH). Exponentially growing cells were collected for TPA treatment by centrifugation at 500 × g for 5 min at 4°C, and the culture medium was then replaced with fresh medium. A total of 2.5×10^6 cells were resuspended in 10 mL of fresh culture medium and cultured in 10-cm dishes. Cells were exposed to 0.2 µg/mL TPA for 24 h at 37°C, whereas vehicle controls received an equivalent volume of 100% EtOH to give a final concentration of 1% (v/v). At the end of the 24-h exposure, cells were collected by centrifugation at 500 × g for 5 min at 4°C and washed twice with 20 mL of fresh culture medium. Cells were resuspended in fresh culture medium and counted after the

final wash. Day 0 was defined as the time point immediately after completion of the 24-h treatment and washing. The cells were subsequently maintained in TPA-free medium and collected on Days 3 and 7 for the analyses described below.

RNA-seq library preparation and sequencing

Total RNA was isolated with the NucleoSpin RNA Plus kit (Macherey-Nagel) according to the manufacturer's instructions. A NanoDrop spectrophotometer was used to measure RNA concentration. Samples containing ≥ 1 μg of total RNA at ≥ 20 ng/μL were sent to Macrogen Japan for library preparation and sequencing. Using the TruSeq Stranded mRNA Library Prep Kit (Illumina, San Diego, CA, USA), RNA-seq libraries were prepared according to the manufacturer's protocol. Libraries were then sequenced on an Illumina NovaSeq X Plus system in paired-end mode with 100-bp reads.

RNA-seq data analysis

FASTQ file quality was assessed using FastQC (v0.12.1, --nogroup) [34]. Adapter sequences and low-quality bases were removed with Trimmomatic (v0.39) in paired-end mode using the following parameters: ILLUMINACLIP:TruSeq3-PE.fa:2:30:10:2:true, SLIDINGWINDOW:4:15, LEADING:3, TRAILING:3, and MINLEN:36 [35]. Trimmed-read quality was then reassessed using FastQC. Trimmed paired-end reads were mapped to the human reference genome (hg19) with HISAT2 (v2.2.1) using default parameters [36]. The resulting alignments were sorted, converted to BAM format, and indexed using samtools (v1.24) [37]. Expression of known transcripts was quantified from the mapped BAM files against the NCBI RefSeq gene annotation (hg19.ncbiRefSeq.gtf) using StringTie (v3.0.3, with the -e and -B options; no strand-specific option was specified) [38]. Gene-level (gene_count_matrix.csv) and transcript-level (transcript_count_matrix.csv) count matrices were generated from the resulting Ballgown-format output using prepDE.py, distributed with StringTie [39]. The script was converted from Python 2 to Python 3 using 2to3, with changes limited to print statements and the dictionary iteration method, and was executed in a Python 3 environment. The prepDE.py average read length option (-l) was retained at its default value of 75 bp.

Differentially expressed genes (DEGs) were identified using the edgeR package (v4.10.1) in R (Bioconductor 3.23) [40]. DEGs were identified separately in four comparisons: EtOH Day 0 vs EtOH Day 3, EtOH Day 0 vs TPA Day 0, EtOH Day 0 vs TPA Day 3, and EtOH Day 0 vs TPA Day 7 (n = 2 biological replicates per condition). For each comparison, a DGEList object was created from the columns of the gene count matrix obtained from StringTie corresponding to the four samples of the two groups, and lowly expressed genes were filtered out using the filterByExpr function, which accounts for sample number and library size in each group (default settings: min.count = 10, min.total.count = 15) [41]. After filtering, library sizes were recalculated and normalized using the trimmed mean of M-values (TMM) method (calcNormFactors) [42]. Dispersion for each gene was then estimated using estimateDisp with a two-group design matrix, a generalized linear model was fitted using glmQLFit, and differential

expression between the two groups was tested using glmQLFTest (quasi-likelihood F-test) [41]. Genes with $log_2FC > 1$ and a nominal (uncorrected) P-value < 0.05 were defined as upregulated, whereas genes with $log_2FC < -1$ and a nominal P-value < 0.05 were defined as downregulated; these genes were extracted as DEGs_UP and DEGs_DOWN, respectively, for each comparison.

For DEG visualization, volcano plots were generated with the base R plot function using log_2FC and $-log_{10}$(P-value) as the axes; dashed lines indicate $|log_2FC| = 1$ and P = 0.05. For the union of upregulated and downregulated DEGs identified across the four comparisons, a DGEList object was created in edgeR (v4.10.1), library sizes were normalized by the TMM method using calcNormFactors, and counts were converted to log_2-CPM values with the cpm function (normalized.lib.sizes = TRUE, log = TRUE, prior.count = 1). The resulting TMM-normalized log_2-CPM values were Z-score standardized for each gene using the genescale function of the genefilter package (v1.94.0; method = "Z"). These values were then input into the heatmap.2 function of the gplots R package (v3.3.0) to generate a heatmap with hierarchical clustering of both genes and samples using Euclidean distance and complete linkage, the default heatmap.2 settings.

Gene Ontology analysis

Gene Ontology (GO) Biological Process (BP) enrichment analysis was performed with the web-based g:Profiler tool (g:GOSt, https://biit.cs.ut.ee/gprofiler/gost; version e114_eg62_p19_27110d83). The DEGs_UP and DEGs_DOWN lists from the EtOH Day 0 vs. TPA Day 0, EtOH Day 0 vs. TPA Day 3, and EtOH Day 0 vs. TPA Day 7 comparisons were submitted separately to g:Profiler. *Homo sapiens* was selected as the organism, the annotation source was restricted to GO:BP, and term size was capped at 1000. Statistical significance was evaluated using g:Profiler's default g:SCS multiple-testing correction, with GO:BP terms considered significant at an adjusted P-value < 0.05. The statistical domain scope remained at the default setting (only annotated genes).

ATAC-seq library preparation and sequencing

Each sample containing 1×10^6 cells was collected by centrifugation at 500 × g for 5 min at 4°C and washed with cold 0.04% bovine serum albumin/PBS. For lysis, cells were incubated on ice for 3 min in 100 µL of ATAC lysis buffer containing 10 mM Tris-HCl (pH 7.5), 10 mM NaCl, 3 mM $MgCl_2$, 0.1% Tween-20, 0.1% NP-40, and 0.01% digitonin. ATAC wash buffer containing 0.1% Tween-20 was then added, after which nuclei were counted with a hemocytometer. A total of 5×10^4 nuclei were recovered by centrifugation at 500 × g for 10 min at 4°C and resuspended in 47.8 µL of ATAC reaction buffer containing 10 mM Tris-HCl (pH 7.6), 5 mM $MgCl_2$, 10% N,N-dimethylformamide, PBS, 0.01% digitonin, and 0.2% Tween-20. Following addition of 2.2 µL adapter-loaded Tn5 transposase, the transposition reaction proceeded for 30 min at 37°C. The resulting DNA was purified with the MinElute PCR Purification Kit (Qiagen, Hilden, Germany). Initial amplification of transposed DNA was carried out in a 50-µL PCR containing 20 µL purified DNA, 25 µL 2× KAPA HiFi HotStart ReadyMix (Kapa Biosystems), and unique dual-index primers containing Nextera-compatible i5 and i7 adapter sequences. PCR was

performed at 72°C for 5 min and 98°C for 30 s, followed by five cycles at 98°C for 10 s, 63°C for 30 s, and 72°C for 1 min. Quantitative PCR with SYBR Green fluorescence was used to determine the number of additional amplification cycles. The cycle corresponding to one-third of the maximum fluorescence intensity was selected, resulting in two additional cycles under the present conditions. Amplified libraries were first purified with the MinElute PCR Purification Kit and then subjected to 1.8× AMPure XP magnetic bead purification (Beckman Coulter) to remove primer dimers. Fragment-size distributions were evaluated on a 4150 TapeStation System using the High Sensitivity D1000 assay (Agilent Technologies), and library concentrations were measured by quantitative PCR with the KAPA Library Quantification Kit according to the manufacturer's instructions. Novogene sequenced the libraries on an Illumina NovaSeq X Plus system in paired-end mode (2 × 150 bp), with 6 Gb targeted per library.

ATAC-seq data analysis

FASTQ file quality was assessed using FastQC (v0.12.1, --nogroup) [34]. Adapter sequences and low-quality bases were removed with Trimmomatic (v0.39) in paired-end mode using the following parameters: ILLUMINACLIP:NexteraPE-PE_ATAC.fa:2:30:10, SLIDINGWINDOW:4:15, LEADING:20, TRAILING:20, and MINLEN:36 [35]. Trimmed-read quality was then reassessed using FastQC. Trimmed paired-end reads were mapped to the human reference genome (hg19) with Bowtie2 (v2.5.5) using default parameters [43]. The resulting alignments were converted to BAM format, sorted, and indexed using samtools (v1.24). PCR duplicate reads were removed with MarkDuplicates in GATK (v4.2.0.0) using the --REMOVE_DUPLICATES option [44], and insert-size metrics were collected using GATK CollectInsertSizeMetrics. Tn5 transposase insertion sites in the duplicate-removed BAM files were shift-corrected with alignmentSieve in deepTools (v3.5.6) using the --ATACshift option to generate shift-corrected BAM files for visualization [45]. Peaks were called from the duplicate-removed, pre-shift-correction BAM files using MACS2 (v2.2.9.1) in BAMPE mode with a q-value cutoff of 0.05 (-q 0.05) and an effective genome size of -g hs to detect open chromatin regions (narrowPeak) for each sample [46]. For each sample, chromosome, start, and end coordinates (chr, start, end) from the narrowPeak files were pooled and sorted (sort -k1,1 -k2,2n); overlapping regions across all samples were then merged with bedtools (v2.31.1) merge to generate a consensus peak set [47]. The resulting BED file was converted to GTF format (feature type: "region"; gene_id: "chromosome:start-end") using an awk command and used as the reference annotation for subsequent read counting. Peak-level read counts for each sample were calculated with the featureCounts function of the Rsubread package (v2.26.0) in R (v4.6.1) (isGTFAnnotationFile = TRUE, GTF.featureType = "region", isPairedEnd = TRUE), using the duplicate-removed BAM files and the consensus peak GTF described above to generate a count matrix. Differentially accessible regions (DARs) were identified with the edgeR package (v4.10.1) in R (Bioconductor 3.23) [40]. Three comparisons were analyzed separately: EtOH Day 0 vs. TPA Day 0, EtOH Day 0 vs. TPA Day 3, and EtOH Day 0 vs. TPA Day 7 (n = 2 biological replicates per condition). For each comparison, a DGEList object was created from the count-matrix columns corresponding to the four samples in the two groups, and lowly accessible regions were filtered using filterByExpr, which accounts for sample number and library size in each group (default settings: min.count = 10, min.total.count = 15)

[41]. After filtering, library sizes were recalculated and normalized by the TMM method using calcNormFactors [42]. Dispersion for each region was estimated with estimateDisp using a two-group design matrix, followed by generalized linear model fitting with glmQLFit and differential-accessibility testing with glmQLFTest (quasi-likelihood F-test). Regions with $\log_2$FC > 1 and a nominal (uncorrected) P-value < 0.05 were defined as regions with increased accessibility (OPEN DARs), whereas regions with $\log_2$FC < -1 and a nominal P-value < 0.05 were defined as regions with decreased accessibility (CLOSE DARs). The nominal P-value, rather than the multiple-testing-corrected FDR, was used as the threshold. For DAR visualization, volcano plots were generated with the base R plot function using $\log_2$FC and -$\log_{10}$(P-value) as the axes; dashed lines indicate |$\log_2$FC| = 1 and P = 0.05. For the union of DARs identified across the three comparisons, a DGEList object was created using edgeR (v4.10.1), library sizes were normalized by the TMM method using calcNormFactors, and counts were converted to $\log_2$-CPM values using the cpm function (normalized.lib.sizes = TRUE, log = TRUE, prior.count = 1). The resulting TMM-normalized $\log_2$-CPM values were Z-score standardized for each region using the genescale function of the genefilter package (v1.94.0; method = "Z"). These values were then input into the heatmap.2 function of the gplots R package (v3.3.0) to generate a heatmap with hierarchical clustering of both regions and samples using Euclidean distance and complete linkage, the default heatmap.2 settings. DARs were annotated to genes using the annotatePeak function of the ChIPseeker R package (v1.48.0) [48]. Based on DAR coordinates, the nearest gene to each region was assigned using TxDb.Hsapiens.UCSC.hg19.knownGene (v3.2.2) as the reference annotation, with the promoter region defined as ± 3000 bp from the transcription start site (tssRegion = c(-3000, 3000)). Gene symbols were assigned using org.Hs.eg.db (v3.23.1), yielding lists of DAR-associated genes for OPEN and CLOSE DARs in each comparison.

Results and Discussion

TPA induces sustained transcriptomic alterations associated with inflammatory responses in TK6 cells

To characterize the global transcriptional response to TPA as a chemical model of inflammatory stimulation, we first examined temporal changes in gene expression in TK6 cells. Cells were treated with TPA for 24 h and collected either immediately after treatment (Day 0) or after TPA removal and recovery culture for 3 or 7 days (Days 3 and 7, respectively) for RNA-seq analysis (Fig. 1A). To evaluate potential vehicle effects on inflammatory responses, ethanol-treated control cells were analyzed on Days 0 and 3. Hierarchical clustering of RNA-seq profiles revealed distinct expression patterns among vehicle-treated cells, cells collected immediately after TPA exposure, and cells in the post-exposure recovery period (Fig. 1B). The transcriptional profile immediately after the 24-h TPA exposure (Day 0) differed from those observed on Days 3 and 7. By contrast, Day 3 and Day 7 samples showed broadly similar expression patterns, which suggests the emergence of a transcriptional state characteristic of the post-exposure period. These observations indicate that the transcriptional effects of TPA are temporally dynamic and extend beyond the period of direct exposure. The distinct expression profiles during recovery may reflect

secondary cellular responses or transcriptional reprogramming initiated by TPA exposure [49]. Ethanol-treated control cells, however, showed only modest transcriptional changes between Days 0 and 3, with no apparent activation of inflammation-related genes. Thus, EtOH Day 0 was used as the common baseline reference to characterize temporal molecular changes following TPA exposure.

Next, we examined temporal changes in differentially expressed genes (DEGs) and their associated biological processes. Immediately after TPA exposure (Day 0), we found that 278 genes were upregulated and 253 were downregulated. During the post-exposure period, the number of upregulated genes increased to 367 on Day 3 and 393 on Day 7, whereas the number of downregulated genes decreased to 157 and 139, respectively (Fig. 1C–E). Thus, although the total number of DEGs remained relatively similar across the three time points, the transcriptional response progressively shifted toward gene upregulation. Gene Ontology (GO) analysis further showed marked temporal changes in the biological processes associated with these DEGs. On Day 0, upregulated genes were enriched in immune- and inflammation-related processes, including regulation of cell activation, positive regulation of immune response, inflammatory response, cytokine production, and lymphocyte activation, whereas downregulated genes showed no significant enrichment of immune- or inflammation-related GO terms. On Day 3, upregulated genes showed broader enrichment of immune-related processes, including leukocyte and lymphocyte activation, T-cell activation, cytokine production, and regulation of cytokine production. By contrast, downregulated genes were enriched in inflammatory and adaptive immune responses together with several signaling and metabolic processes. On Day 7, we observed enrichment of leukocyte, lymphocyte, and T-cell activation and cytokine production among upregulated genes, whereas downregulated genes were associated with regulation of leukocyte and lymphocyte activation, antigen processing and presentation, and cell proliferation. Taken together, these findings suggest that the transcriptional response to TPA evolves from an immediate response into a predominantly upregulated immune- and inflammation-associated program during the post-exposure period [50–52]. The presence of immune-related GO terms in both up- and downregulated gene sets at later time points further indicates that TPA does not simply activate inflammatory transcription globally; instead, it induces coordinated reorganization of immune- and inflammation-related gene expression programs.

TPA induces dynamic genome-wide changes in chromatin accessibility

We next examined whether the transcriptional responses following TPA exposure were accompanied by changes in chromatin accessibility. ATAC-seq was performed with two biological replicates (#1 and #2) per condition, and hierarchical clustering showed closely related accessibility profiles between replicate samples, indicating good within-condition reproducibility (Fig. 2A). Profiles on Days 3 and 7 were broadly similar to each other but differed from those observed immediately after TPA exposure. To directly compare temporal changes across the RNA-seq and ATAC-seq datasets, EtOH Day 0 was used as a common baseline. Differentially accessible region (DAR) analysis revealed extensive, time-dependent changes in chromatin accessibility following TPA exposure (Fig. 2B–D). Immediately after the 24-h treatment, 5,241 regions showed increased accessibility (open DARs), whereas 1,247 showed decreased

accessibility (closed DARs). During the post-exposure period, the number of altered regions increased to 7,655 open and 3,709 closed DARs on Day 3 and 8,143 open and 4,567 closed DARs on Day 7. Accordingly, the total number of DARs rose from 6,488 on Day 0 to 11,364 on Day 3 and 12,710 on Day 7, with regions of increased accessibility consistently outnumbering those of decreased accessibility. These results indicate that the chromatin state progressively diverged during the post-exposure period rather than rapidly returning to the pre-exposure state after TPA removal. The continued expansion of baseline-relative DARs on Days 3 and 7 further suggests that chromatin remodeling is temporally dynamic and extends beyond direct chemical exposure [53]. Together with the time-dependent transcriptional changes described above, these results provided the basis for subsequent integrated analysis of gene expression and chromatin accessibility.

Integrated RNA-seq and ATAC-seq analyses identify concordant changes associated with inflammatory responses

Next, we integrated the RNA-seq and ATAC-seq datasets and classified differentially expressed genes according to the presence of directionally concordant accessibility changes to determine the extent to which TPA-induced transcriptional changes were accompanied by altered chromatin accessibility. Upregulated genes associated with open DARs and downregulated genes associated with closed DARs were defined as concordant DEG–DAR genes. Of the 278 upregulated genes detected on Day 0, 91 (32.7%) were associated with increased chromatin accessibility, whereas 187 showed transcriptional changes without corresponding open DARs (Fig. 3A) (Table S1). The proportion of concordant upregulated genes increased to 184 of 367 genes (50.1%) on Day 3 and remained relatively high on Day 7 (Fig. 3B–C), when 182 of 393 genes (46.3%) showed concordant increases in expression and chromatin accessibility. Downregulated genes showed a more pronounced temporal increase in concordance. Only 22 of 253 downregulated genes (8.7%) were associated with closed DARs on Day 0 (Fig. 3D), but this proportion increased to 41 of 157 genes (26.1%) on Day 3 and 55 of 139 genes (39.6%) on Day 7 (Fig. 3E–F). These results indicate that coupling between transcriptional change and chromatin accessibility becomes more prominent during the post-exposure period, particularly for transcriptional repression.

We next performed Gene Ontology analysis on the concordant gene sets to determine whether coordinated transcriptional and chromatin-accessibility changes mapped to coherent biological processes (Table S2). On Day 0, concordant upregulated genes were enriched in immune- and inflammation-related processes, including leukocyte activation, inflammatory response, cytokine-mediated signaling pathway, and cellular response to molecules of bacterial origin (Fig. 3A). By Day 3, the enriched terms had broadened to include leukocyte and lymphocyte activation, T-cell activation, cytokine production, regulation of cytokine production, and MAPK signaling (Fig. 3B). Concordant upregulated genes on Day 7 continued to show enrichment in leukocyte activation, cytokine production, regulation of cell activation, and receptor-mediated signaling (Fig. 3C). In contrast, the small set of

concordant downregulated genes on Day 0 showed no significant GO enrichment (Fig. 3D). Concordant downregulated genes were associated with metabolic processes on Day 3 and with regulation of T-cell, lymphocyte, and leukocyte activation on Day 7 (Fig. 3E–F). Directionally concordant chromatin-accessibility changes therefore accompanied a larger proportion of DEGs during the post-exposure period than immediately after TPA treatment, with the strongest temporal increase observed among downregulated genes.

Partial concordance between gene expression and chromatin accessibility further illustrates the regulatory heterogeneity of the chemical response. Many DEGs underwent significant transcriptional change without a detectable corresponding change in accessibility. Several mechanisms could generate these RNA-only responses: transcription may originate from regulatory regions that were already accessible before TPA exposure; transcription factor activity or histone modifications may change without major accessibility changes [54]; distal regulatory elements may not have been assigned to the corresponding gene [55]; or regulation may occur post-transcriptionally. Conversely, concordant increases or decreases in expression and accessibility define a more restricted gene subset in which transcriptional responses are accompanied by detectable remodeling of the local chromatin environment.

This distinction is particularly relevant to the present study because it provides information unavailable from RNA-seq alone. Transcriptomic analysis identifies genes whose expression responds to chemical exposure, whereas integration with ATAC-seq identifies genes for which that transcriptional response is accompanied by a coordinated change in chromatin accessibility. The progressive increase in concordance during recovery suggests that chromatin remodeling may contribute increasingly to establishment or maintenance of the post-exposure transcriptional state. Although this association does not establish a causal relationship between accessibility and transcription, it identifies a subset of genes showing coordinated regulation at two molecular levels [9]. Such concordant genes may therefore be particularly informative candidates for evaluating chemically induced inflammatory effects because they reflect both transcriptional output and an associated change in chromatin state.

Concordant RNA–ATAC changes in disease-associated inflammatory genes

We next focused on the temporal behavior of concordant genes that had previously been linked to susceptibility to or pathogenesis of inflammatory diseases. Among 184 concordant upregulated/open genes detected on Day 3, 115 remained concordant on Day 7 and 67 additional genes newly acquired both upregulation and increased accessibility on Day 7. Of the 41 concordant downregulated/closed genes detected on Day 3, 24 remained concordant on Day 7, while another 31 genes newly entered this category (Fig. 4A and B). Thus, many concordant responses present on Day 3 persisted through Day 7, while a second group of genes developed coordinated transcriptional and chromatin-accessibility changes later during recovery.

We then examined specific concordant genes with established associations with human inflammatory or immune-mediated diseases. IGV was used to visualize representative immune- and inflammation-related genes showing coordinated expression and accessibility changes. *TNFSF4, CSF2, and SELL* were selected because prominent accessibility changes occurred near their transcription start sites together with corresponding changes in transcript abundance (Fig. 4C–E). *TNFSF4* encodes OX40L and is particularly relevant because variants at this locus have been associated with susceptibility to systemic lupus erythematosus; the disease-associated risk haplotype has also been linked to increased *TNFSF4* expression [56]. *CSF2* encodes GM-CSF, an important regulator of inflammatory myeloid responses whose dysregulation has been implicated in autoimmune and inflammatory diseases including rheumatoid arthritis and multiple sclerosis [57]. Following TPA exposure, *SELL*, which encodes the leukocyte adhesion molecule L-selectin (CD62L), was downregulated, consistent with sustained reprogramming of leukocyte adhesion and trafficking pathways during inflammatory activation. Reduced L-selectin expression has likewise been reported in inflammatory disorders, including systemic inflammatory response syndrome/sepsis and severe psoriasis [58, 59]. Thus, TPA exposure produced coordinated transcriptional and local chromatin-accessibility changes at these disease-associated inflammatory genes. Such responses may constitute molecular signatures of chemically induced inflammatory toxicity and provide candidate indicators for evaluation of inflammation-related toxic effects.

Integrating the two datasets may therefore provide information beyond transcript abundance alone. RNA-seq captures the transcriptional output of chemical exposure, while a concurrent accessibility change indicates remodeling of the local chromatin environment associated with that output. At disease-associated inflammatory genes, concordant RNA–ATAC responses consequently form a two-layer molecular signature comprising both transcriptional and chromatin changes. These genes may be especially informative as candidate indicators of chemically induced inflammatory effects because altered expression can be linked to a detectable change in the underlying regulatory chromatin state. The present results do not show that chemical exposure itself confers disease risk, nor do they establish these genes as validated biomarkers. Instead, they indicate that coordinated transcriptional and chromatin responses at genes already implicated in human inflammatory disease could be used to prioritize candidate molecular indicators of inflammatory hazard. Whether such concordant signatures can be generalized for chemical hazard assessment will require validation across additional chemicals and exposure conditions.

Conclusions

By integrating transcriptomic and chromatin-accessibility profiling, this study demonstrates an approach for assessing chemically induced inflammatory effects at two molecular levels. In human TK6 cells, TPA caused time-dependent changes in gene expression together with genome-wide changes in chromatin accessibility. Integration of the RNA-seq and ATAC-seq datasets identified genes for which these responses were concordant, including genes associated with inflammatory and immune-related processes and with human disease susceptibility. Concordant RNA–ATAC changes may therefore

provide information beyond conventional transcriptomic endpoints because they capture both the functional transcriptional output of chemical exposure and an accompanying change in chromatin state. TK6 cells are particularly suitable for this strategy because they are a well-characterized human model used extensively in chemical safety assessment and can provide a common experimental platform for extending conventional genotoxicity testing to non-genotoxic and epigenomic effects. Additional chemicals, exposure conditions, and larger datasets will be needed for validation. Nevertheless, the present approach provides a foundation for developing disease- and inflammation-associated concordant molecular signatures as candidate indicators of chemically induced biological effects and for advancing mechanistically informed chemical safety assessment.

Abbreviations

ATAC-seq: assay for transposase-accessible chromatin using sequencing **BP**: biological process **cGAS–STING**: cyclic GMP–AMP synthase–stimulator of interferon genes **CPM**: counts per million **DARs**: differentially accessible regions **DEGs**: differentially expressed genes **EtOH**: ethanol **FDR**: false discovery rate **GO**: Gene Ontology **JAK–STAT**: Janus kinase–signal transducer and activator of transcription **NF-κB**: nuclear factor kappa B **PBS**: phosphate-buffered saline **RNA-seq**: RNA sequencing **TMM**: trimmed mean of M-values **TPA**: 12-O-tetradecanoylphorbol-13-acetate

Declarations

Ethics approval and consent to participate

Not applicable

Consent for publication

Not applicable

Competing interests

The authors declare that they have no competing interests to disclose.

Authors’ information

Not applicable.

Funding

This work was supported by the Consumer Affairs Agency, Government of Japan (Grant Number 24KA1008), the Ministry of Health, Labour and Welfare of Japan (Grant Number 21KA1001), and JSPS

KAKENHI (Grant Number 22H03748). Additional funding was provided by grants from the Takeda Science Foundation [to A.S.].

Author Contribution

KY, MY, MH, KS, RF, AK, KU, and AS designed the research and discussed the study. KY, RF, and AS performed the experiments and analyzed the data. KY and AS drafted the manuscript. All authors read and approved the final manuscript.

Acknowledgement

The authors thank Mr. Ken Takafuji and Mr. Yuanzhe Cui (Chiba University) for their technical assistance.

Availability of data and materials

All RNA-seq and ATAC-seq datasets generated in this study were deposited in the DDBJ under BioProject accession numbers PRJDB45770 and PRJDB45772, respectively.

References

1. Phillips DH, Arlt VM. Genotoxicity: damage to DNA and its consequences. EXS. 2009;99:87–110.
2. Yamada H, Odagiri M, Yamakita K, Chiba A, Ukai A, Yasui M, Honma M, Sugiyama KI, Ura K, Sassa A. Dual-directional epi-genotoxicity assay for assessing chemically induced epigenetic effects utilizing the housekeeping TK gene. Sci Rep. 2025;15:7780.
3. Herceg Z, Lambert MP, van Veldhoven K, Demetriou C, Vineis P, Smith MT, Straif K, Wild CP. Towards incorporating epigenetic mechanisms into carcinogen identification and evaluation. Carcinogenesis. 2013;34:1955–67.
4. Desaulniers D, Vasseur P, Jacobs A, Aguila MC, Ertych N, Jacobs MN. Integration of Epigenetic Mechanisms into Non-Genotoxic Carcinogenicity Hazard Assessment: Focus on DNA Methylation and Histone Modifications. Int J Mol Sci 2021, 22.
5. Jirtle RL, Skinner MK. Environmental epigenomics and disease susceptibility. Nat Rev Genet. 2007;8:253–62.
6. Lu C, Thompson CB. Metabolic regulation of epigenetics. Cell Metab. 2012;16:9–17.
7. Kaelin WG Jr., McKnight SL. Influence of metabolism on epigenetics and disease. Cell. 2013;153:56–69.
8. Soria G, Polo SE, Almouzni G. Prime, repair, restore: the active role of chromatin in the DNA damage response. Mol Cell. 2012;46:722–34.

9. Klemm SL, Shipony Z, Greenleaf WJ. Chromatin accessibility and the regulatory epigenome. Nat Rev Genet. 2019;20:207–20.
10. Medzhitov R, Horng T. Transcriptional control of the inflammatory response. Nat Rev Immunol. 2009;9:692–703.
11. Coussens LM, Werb Z. Inflammation and cancer. Nature. 2002;420:860–7.
12. Chung FF, Herceg Z. The Promises and Challenges of Toxico-Epigenomics: Environmental Chemicals and Their Impacts on the Epigenome. Environ Health Perspect. 2020;128:15001.
13. Takeuchi O, Akira S. Pattern recognition receptors and inflammation. Cell. 2010;140:805–20.
14. West AP, Shadel GS. Mitochondrial DNA in innate immune responses and inflammatory pathology. Nat Rev Immunol. 2017;17:363–75.
15. Hopfner KP, Hornung V. Molecular mechanisms and cellular functions of cGAS-STING signalling. Nat Rev Mol Cell Biol. 2020;21:501–21.
16. Schonthaler HB, Guinea-Viniegra J, Wagner EF. Targeting inflammation by modulating the Jun/AP-1 pathway. Ann Rheum Dis. 2011;70(Suppl 1):i109–112.
17. Morgan MJ, Liu ZG. Crosstalk of reactive oxygen species and NF-kappaB signaling. Cell Res. 2011;21:103–15.
18. Smolen JS, Aletaha D, Barton A, Burmester GR, Emery P, Firestein GS, Kavanaugh A, McInnes IB, Solomon DH, Strand V, Yamamoto K. Rheumatoid arthritis. Nat Rev Dis Primers. 2018;4:18001.
19. Franceschi C, Campisi J. Chronic inflammation (inflammaging) and its potential contribution to age-associated diseases. J Gerontol Biol Sci Med Sci. 2014;69(Suppl 1):S4–9.
20. Ramantani G, Kohlhase J, Hertzberg C, Innes AM, Engel K, Hunger S, Borozdin W, Mah JK, Ungerath K, Walkenhorst H, et al. Expanding the phenotypic spectrum of lupus erythematosus in Aicardi-Goutieres syndrome. Arthritis Rheum. 2010;62:1469–77.
21. Cano-Gamez E, Trynka G. From GWAS to Function: Using Functional Genomics to Identify the Mechanisms Underlying Complex Diseases. Front Genet. 2020;11:424.
22. Calderon D, Nguyen MLT, Mezger A, Kathiria A, Muller F, Nguyen V, Lescano N, Wu B, Trombetta J, Ribado JV, et al. Landscape of stimulation-responsive chromatin across diverse human immune cells. Nat Genet. 2019;51:1494–505.
23. Farh KK, Marson A, Zhu J, Kleinewietfeld M, Housley WJ, Beik S, Shoresh N, Whitton H, Ryan RJ, Shishkin AA, et al. Genetic and epigenetic fine mapping of causal autoimmune disease variants. Nature. 2015;518:337–43.
24. Glass CK, Natoli G. Molecular control of activation and priming in macrophages. Nat Immunol. 2016;17:26–33.
25. Netea MG, Dominguez-Andres J, Barreiro LB, Chavakis T, Divangahi M, Fuchs E, Joosten LAB, van der Meer JWM, Mhlanga MM, Mulder WJM, et al. Defining trained immunity and its role in health and disease. Nat Rev Immunol. 2020;20:375–88.

26. Kuroki S, Yamada H, Odagiri M, Sugiyama KI, Yasui M, Sassa A. Quantifying Epigenetic Changes Induced by Chemical Exposure Using the epi-TK Assay. Bio Protoc. 2026;16:e5671.
27. Yasui M, Fukuda T, Ukai A, Maniwa J, Imamura T, Hashizume T, Yamamoto H, Shibuya K, Narumi K, Fujiishi Y, et al. Weight of evidence approach using a TK gene mutation assay with human TK6 cells for follow-up of positive results in Ames tests: a collaborative study by MMS/JEMS. Genes Environ. 2021;43:7.
28. Sassa A, Fukuda T, Ukai A, Nakamura M, Takabe M, Takamura-Enya T, Honma M, Yasui M. Comparative study of cytotoxic effects induced by environmental genotoxins using XPC- and CSB-deficient human lymphoblastoid TK6 cells. Genes Environ. 2019;41:15.
29. Sassa A, Fukuda T, Ukai A, Nakamura M, Sato R, Fujiwara S, Hirota K, Takeda S, Sugiyama KI, Honma M, Yasui M. Follow-up genotoxicity assessment of Ames-positive/equivocal chemicals using the improved thymidine kinase gene mutation assay in DNA repair-deficient human TK6 cells. Mutagenesis. 2021;36:331–8.
30. Griner EM, Kazanietz MG. Protein kinase C and other diacylglycerol effectors in cancer. Nat Rev Cancer. 2007;7:281–94.
31. Medeiros R, Otuki MF, Avellar MC, Calixto JB. Mechanisms underlying the inhibitory actions of the pentacyclic triterpene alpha-amyrin in the mouse skin inflammation induced by phorbol ester 12-O-tetradecanoylphorbol-13-acetate. Eur J Pharmacol. 2007;559:227–35.
32. Cataisson C, Pearson AJ, Torgerson S, Nedospasov SA, Yuspa SH. Protein kinase C alpha-mediated chemotaxis of neutrophils requires NF-kappa B activity but is independent of TNF alpha signaling in mouse skin in vivo. J Immunol. 2005;174:1686–92.
33. Honma M, Izumi M, Sakuraba M, Tadokoro S, Sakamoto H, Wang W, Yatagai F, Hayashi M. Deletion, rearrangement, and gene conversion; genetic consequences of chromosomal double-strand breaks in human cells. Environ Mol Mutagen. 2003;42:288–98.
34. A quality control. tool for high throughput sequence data. [https://www.bioinformatics.babraham.ac.uk/projects/fastqc/]
35. Bolger AM, Lohse M, Usadel B. Trimmomatic: a flexible trimmer for Illumina sequence data. Bioinformatics. 2014;30:2114–20.
36. Kim D, Paggi JM, Park C, Bennett C, Salzberg SL. Graph-based genome alignment and genotyping with HISAT2 and HISAT-genotype. Nat Biotechnol. 2019;37:907–15.
37. Danecek P, Bonfield JK, Liddle J, Marshall J, Ohan V, Pollard MO, Whitwham A, Keane T, McCarthy SA, Davies RM, Li H. Twelve years of SAMtools and BCFtools. *Gigascience* 2021, 10.
38. Pertea M, Pertea GM, Antonescu CM, Chang TC, Mendell JT, Salzberg SL. StringTie enables improved reconstruction of a transcriptome from RNA-seq reads. Nat Biotechnol. 2015;33:290–5.
39. Pertea M, Kim D, Pertea GM, Leek JT, Salzberg SL. Transcript-level expression analysis of RNA-seq experiments with HISAT, StringTie and Ballgown. Nat Protoc. 2016;11:1650–67.
40. Robinson MD, McCarthy DJ, Smyth GK. edgeR: a Bioconductor package for differential expression analysis of digital gene expression data. Bioinformatics. 2010;26:139–40.

41. Chen Y, Lun AT, Smyth GK. From reads to genes to pathways: differential expression analysis of RNA-Seq experiments using Rsubread and the edgeR quasi-likelihood pipeline. F1000Res. 2016;5:1438.
42. Robinson MD, Oshlack A. A scaling normalization method for differential expression analysis of RNA-seq data. Genome Biol. 2010;11:R25.
43. Langmead B, Salzberg SL. Fast gapped-read alignment with Bowtie 2. Nat Methods. 2012;9:357–9.
44. McKenna A, Hanna M, Banks E, Sivachenko A, Cibulskis K, Kernytsky A, Garimella K, Altshuler D, Gabriel S, Daly M, DePristo MA. The Genome Analysis Toolkit: a MapReduce framework for analyzing next-generation DNA sequencing data. Genome Res. 2010;20:1297–303.
45. Ramirez F, Ryan DP, Gruning B, Bhardwaj V, Kilpert F, Richter AS, Heyne S, Dundar F, Manke T. deepTools2: a next generation web server for deep-sequencing data analysis. Nucleic Acids Res. 2016;44:W160–165.
46. Zhang Y, Liu T, Meyer CA, Eeckhoute J, Johnson DS, Bernstein BE, Nusbaum C, Myers RM, Brown M, Li W, Liu XS. Model-based analysis of ChIP-Seq (MACS). Genome Biol. 2008;9:R137.
47. Quinlan AR, Hall IM. BEDTools: a flexible suite of utilities for comparing genomic features. Bioinformatics. 2010;26:841–2.
48. Yu G, Wang LG, He QY. ChIPseeker: an R/Bioconductor package for ChIP peak annotation, comparison and visualization. Bioinformatics. 2015;31:2382–3.
49. Bevington SL, Cauchy P, Piper J, Bertrand E, Lalli N, Jarvis RC, Gilding LN, Ott S, Bonifer C, Cockerill PN. Inducible chromatin priming is associated with the establishment of immunological memory in T cells. EMBO J. 2016;35:515–35.
50. Healy S, Khan P, Davie JR. Immediate early response genes and cell transformation. Pharmacol Ther. 2013;137:64–77.
51. Kontny E, Ziolkowska M, Ryzewska A, Maslinski W. Protein kinase c-dependent pathway is critical for the production of pro-inflammatory cytokines (TNF-alpha, IL-1beta, IL-6). Cytokine. 1999;11:839–48.
52. Damascena HL, Silveira WAA, Castro MS, Fontes W. Neutrophil Activated by the Famous and Potent PMA (Phorbol Myristate Acetate). Cells 2022, 11.
53. Ostuni R, Piccolo V, Barozzi I, Polletti S, Termanini A, Bonifacio S, Curina A, Prosperini E, Ghisletti S, Natoli G. Latent enhancers activated by stimulation in differentiated cells. Cell. 2013;152:157–71.
54. Tu Z, Bi Y, Mao T, Wang H, Gao S, Wang Y. Discordance between chromatin accessibility and transcriptional activity during the human primed-to-naive pluripotency transition process. Cell Regen. 2023;12:35.
55. Sanyal A, Lajoie BR, Jain G, Dekker J. The long-range interaction landscape of gene promoters. Nature. 2012;489:109–13.
56. Cunninghame Graham DS, Graham RR, Manku H, Wong AK, Whittaker JC, Gaffney PM, Moser KL, Rioux JD, Altshuler D, Behrens TW, Vyse TJ. Polymorphism at the TNF superfamily gene TNFSF4

confers susceptibility to systemic lupus erythematosus. Nat Genet. 2008;40:83–9.

57. Wicks IP, Roberts AW. Targeting GM-CSF in inflammatory diseases. Nat Rev Rheumatol. 2016;12:37–48.
58. Inaoki M, Sato S, Shimada Y, Kawara S, Steeber DA, Tedder TF, Takehara K. Decreased expression levels of L-selectin on subsets of leucocytes and increased serum L-selectin in severe psoriasis. Clin Exp Immunol. 2000;122:484–92.
59. Ahmed NA, Christou NV. Decreased neutrophil L-selectin expression in patients with systemic inflammatory response syndrome. Clin Invest Med. 1996;19:427–34.

Figures

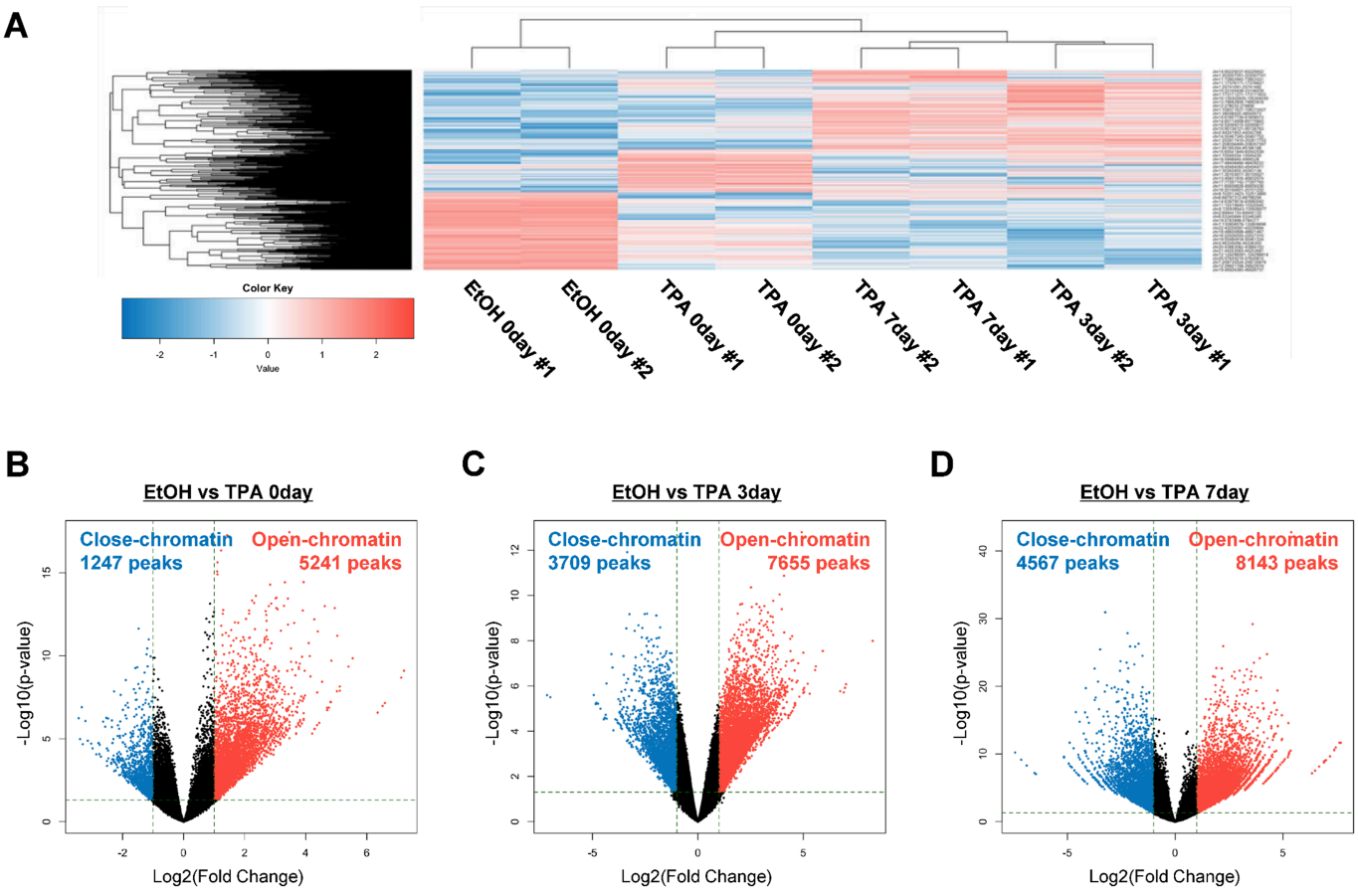


Figure 2

Figure 2

Global chromatin accessibility dynamics following TPA exposure. (A) Hierarchical clustering heatmap of ATAC-seq profiles following TPA exposure. Two biological replicates were analyzed for each

condition. Accessibility values for the union of differentially accessible regions (DARs) were TMM-normalized, converted to log2-CPM, and Z-score standardized for each region. (B–D) Volcano plots showing differential chromatin accessibility at Day 0 (B), Day 3 (C), and Day 7 (D), respectively. EtOH Day 0 was used as the common baseline reference. Regions with log2FC > 1 and P < 0.05 were defined as open DARs, whereas regions with log2FC < −1 and P < 0.05 were defined as closed DARs. The numbers of open and closed DARs are indicated in each panel. Two biological replicates were analyzed per condition.